Journal of Systems Engineering and Electronics
Vol. 31, No. 6, December 2020, pp.1262 – 1273

Accurate estimation of line-of-sight rate under strong impact interference effect

ZHOU Di*, HU Zhiheng, and ZHANG Wenxue

School of Astronautics, Harbin Institute of Technology, Harbin 150001, China

Abstract: In the process of the terminal guidance of a kinetic kill vehicle (KKV), it is very important to accurately estimate the line-of-sight (LOS) rate via the measurements of a target seeker onboard the KKV. The strong impact interference caused by the large lateral thrust produced by the thrusters on the KKV is a main factor that affects the measurements on the LOS angle. A method to estimate the impact interference and the LOS rate together via a Kalman filter is proposed to improve the estimation precision of the LOS rate. The observability of the system describing the missile-target relative motion model and the impact interference model is proved, and then a Kalman filter is designed. In the Kalman filter design, the continuous-discrete and two-stage filtering techniques are used because the system model is time-variant and high-order. Numerical simulation results show that by estimating the impact interference, the estimation precision of the LOS rate is increased, and so the miss distance of the KKV under the strong impact interference is reduced. The proposed continuous-discrete two-stage Kalman filter shows higher estimation precision and lower computational cost than the naive discrete augmented state Kalman filter.

Keywords: guidance, impact interference, linear time-variant system, observability, continuous-discrete Kalman filter, two-stage Kalman filter.

DOI: 10.23919/JSEE.2020.000097

1. Introduction

To intercept a target precisely, during the terminal guidance phase of a kinetic kill vehicle (KKV), the target-missile line-of-sight (LOS) rate must be accurately estimated. This is essential to any terminal guidance law. How to precisely estimate the value of LOS rate from a target seeker's measurements is a very important topic. A strapdown seeker is commonly applied in the guidance system of the KKV. It is mounted on the missile body rigidly, providing some advantages [1], such as compact structure, low cost and so on. On the other hand, the LOS angles cannot be measured directly. The output of the seeker is the body LOS angle, which is coupled with the body attitude motion. The coupling increases the difficulty in LOS rate estimation, making it a key issue for strapdown guidance applications. In such a strapdown seeker system, the LOS angles are usually calculated out by utilizing the missile body's attitude information acquired from the inertial measurement unit (IMU).

The estimation of LOS rate for strapdown seekers has been studied in recent years. Main methods are additive rate compensation [2] and variants of Kalman filters [3-8]. In the additive rate compensation method, attitude information from the IMU is introduced into the tracking loop to cancel out the influence of the body attitude. Du et al. [2] introduced an integrated compensation method that consists of the additive rate compensation method for body disturbance, the cross-decoupling method for rolling movement, and the angle-compensation method for tracking loop dynamic lag to calculate the real LOS rate of a rolling interceptor. In the Kalman filter method, a model including body attitude and real LOS rate is established, from which the LOS rate is estimated via nonlinear Kalman filter algorithms. Waldmann [3] described the modeling of an imaging seeker and used the extended Kalman filter (EKF) to estimate the LOS rate. Kranthi et al. [4] gave an introduction on the models used in the terminal guidance phase and showed the fast convergence and robustness of EKF. Zhang et al. [5] and Sun et al. [6] estimated the inertial LOS rate using the unscented Kalman filter (UKF) method, which avoids calculating Jacobian matrices in EKF. Wang et al. [7] proposed an extraction method based on the nonlinear tracking differentiator and UKF. Zhang et al. [8] used the particle filter (PF) algorithm which suffers from the high computational load. Wei et al. [9] used fifth-degree cubature Kalman filter (CKF) with an augmented-dimensional model to increase the estimation precision. However, in these articles the impact interference effects on the estimation of LOS rate

Manuscript received May 09, 2019.
*Corresponding author.
This work was supported by the National Natural Science Foundation of China (61773142).

have not been considered.

To intercept a target in the exo-atmosphere, the KKV switches on and off its pulse thrusters to output the desired lateral thrust. In practice, the pulse thrusts produce large impact interference effects on the elastic missile body, resulting in a worse measurement environment for the strapdown seeker. The IMU, which is mounted on the missile body, also suffers from the interference. The flight test of FTG06a occurred in December 2010 failed because of excessive vibration in the IMU [10]. Therefore, the impact interference seriously influences the estimation of LOS rate. However, up to now, there has been few researches about the estimation of LOS rate under the impact interference effects.

A fundamental question that arises when filters are utilized to estimate the state of a system is how to choose a model and measurement function that faithfully captures the system dynamics and guarantees there is sufficient information contained in the measurement to adequately reconstruct the full system dynamics [11]. Observability is an important property of a system which measures this. Lack of observability means that no information can be obtained through the observation. The filter estimate will not converge to a meaning solution or even diverge [12]. However, the observability of the LOS rate has not been discussed in the above references.

The Kalman filter is originally published as a discrete algorithm. In practice, time is naturally continuous but not discrete, and the discretization of state dynamics may be intractable, so the continuous-time version is published later, which is also known as the Kalman-Bucy filter. In engineering, the sensor measurements are usually obtained at discrete time instances. For these reasons, a more realistic approach than discrete-time filtering and continuous-time filtering is continuous-discrete filtering. In continuous-discrete filtering the state dynamics are modeled as continuous-time stochastic processes, and the measurements are obtained at discrete time distances. It avoids the discretization of state dynamics and fits the working condition of sensors.

Nonlinear variants of Kalman filters have also been extended to corresponding continuous-discrete versions. Kulikov et al. [13] proposed an accurate continuous-discrete EKF with global error control. This algorithm is more flexible and robust. Sarkka [14] considered the application of UKF to continuous-discrete filtering problems. Knudsen et al. [15] gave a novel continuous-discrete UKF algorithm simpler than before. Kulikov et al. [16] advanced the idea of accurate Gaussian filtering and gave a square-root implementation of continuous-discrete UKF. Arasaratnam et al. [17] extended the standard CKF, and Santos-Diaz et al. [18] extended the high-degree CKF to continuous-discrete filtering. Wang et al. [19] introduced a stochastic feedback scheme to fix the unpredicted approximation error issue in many filtering problems. He et al. [20] proposed the covariance feedback framework integrated with the continuous-discrete CKF for the bearing-only tracking system. Kulikov et al. [21] presented a mixed-type algorithm, which unifies the features of the accurate continuous-discrete EKF and UKF. Then, they gave a square-root version [22] to fix the numerical issue. Wang et al. [23] extended the accurate idea to the optimal smoothing problem. However, nonlinear models and algorithms are complicated and computationally expensive, and so they do not suit real-time applications such as the guidance process of KKV. Linearization models and algorithms are preferred in practice.

To estimate the error (or bias) in sensor measurements in Kalman filtering, the intuitive method is to treat the error as part of the system state and then estimate the error as well as the system state. This leads to an augmented state Kalman filter (ASKF) whose implementation can be computationally intensive. Friedland [24] proposed to employ a two-stage Kalman filter (TSKF) to decouple the augmented filter into two parallel reduced-order filters. While Friedland's decomposition assumed a constant bias, it is not equivalent to the augmented filter with a dynamical or random error. Hsieh and Chen [25] modified the decoupled filters to fix this issue, and then generalized the two-stage decoupling technique for general linear filtering [26]. This technique has also been applied in nonlinear Kalman filters such as EKF [27] and UKF [28]. It is adopted in practical applications such as fault diagnosis [29,30] and sensor registration [31].

This paper is thus motivated to fill the blanks and apply the techniques listed above. In this paper, we try to design a filter to estimate the impact interference effects to improve the extraction accuracy of the LOS rate. In the design of the filter, we apply continuous-discrete and two-stage filtering techniques for the special structure of the system model. The contributions of this paper can be summarized as follows:

(i) The observability of the impact interference is proved rigorously.

(ii) A Kalman filter is designed to estimate the impact interference effects instead of ignoring them. Through the filter we can compensate the influence of the impact interference effect on the LOS rate.

(iii) To tackle the time-variant and high-order system model, the continuous-discrete and two-stage filtering techniques have been exploited in the design of the filter.

The remainder of this paper is organized as follows. In Section 2, the dynamics of the impact interference of the pulse thruster is modeled as a higher order linear term

and is integrated with the target-missile relative motion dynamics to formulate the augmented state system model. Section 3 gives the proof of the observability of the system. In Section 4, the effect of impact interference is introduced into the Kalman filtering model, after which the continuous-discrete and two-stage filtering techniques are applied. In Section 5, numerical simulations show that by the method of estimating the impact interference, the LOS rate can be more accurately estimated. By using the filter proposed in this paper, the estimation precision can be further improved without too much computational cost increase.

2. Problem formulation

During the terminal guidance phase, it is convenient to choose the initial LOS frame as an inertial frame. This frame is defined as follows. When the terminal guidance phase begins, we select the mass center of the missile as the origin O, the direction pointing to the target along the LOS as the axis Ox, the direction which is upward and perpendicular to Ox in the plumb plane containing Ox as the axis Oy, and the direction forming a right-handed system with Ox and Oy as the axis Oz.

The relative motion between a missile and a target in the 2D plane is shown in Fig. 1.

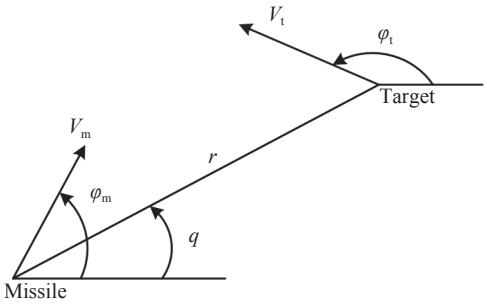

Fig. 1 Relative motion between missile and target in two-dimensional plane

The equation of the relative motion along and perpendicular to the LOS is given by

$$\begin{cases} \dot{r} = V_t \cos(q-\varphi_t) - V_m \cos(q-\varphi_m) \\ r\dot{q} = -V_t \sin(q-\varphi_t) + V_m \sin(q-\varphi_m) \end{cases} \tag{1}$$

where q is the LOS angle; $\dot{q}$ is the LOS rate; r is the relative range from the target to the missile; $\dot{r}$ is the relative velocity, which is usually regarded as a constant in theoretical analysis; V_m and V_t are the missile's velocity and the target's velocity, respectively; φ_m and φ_t are the missile's flight path angle and the target's flight path angle, respectively. By differentiating the both sides of (1) with respect to time, one can get

$$\ddot{q} = -\frac{2\dot{r}}{r}\dot{q} - \frac{1}{r}a_m + \frac{1}{r}a_t \tag{2}$$

where a_m and a_t are the missile's acceleration and target's acceleration respectively.

Choose the state variables as $x_1 = q$, $x_2 = \dot{q}$ and the control input as $u_1 = a_m - a_t$. The differential equation (2) can be written into the following state space form:

$$\begin{cases} \dot{x}_1 = x_2 \\ \dot{x}_2 = -\dfrac{2\dot{r}}{r}x_2 - \dfrac{1}{r}u_1 \end{cases}, \tag{3}$$

or in the matrix form:

$$\dot{\boldsymbol{x}}_1 = \boldsymbol{A}_1(t)\boldsymbol{x}_1 + \boldsymbol{B}_1 u_1 \tag{4}$$

where

$$\boldsymbol{x}_1 = \begin{bmatrix} x_1 \\ x_2 \end{bmatrix}, \boldsymbol{A}_1(t) = \begin{bmatrix} 0 & 1 \\ 0 & -\dfrac{2\dot{r}}{r} \end{bmatrix}, \boldsymbol{B}_1(t) = \begin{bmatrix} 0 \\ -\dfrac{1}{r} \end{bmatrix}. \tag{5}$$

In common case, the decoupled LOS angle measurement is regarded as the input of the filter whose dynamical model is (3), to get the estimate of the LOS rate which is then utilized by the guidance law.

However, because of the impact interference of the pulse thrusters, the seeker and the IMU will vibrate along with the missile body. The attitude of the elastic missile can be approximated as the sum of the rigid body attitude and the additive attitude error produced by the pulse thrusters when only one direction is considered. The dynamic characteristic of the elastic missile is usually acquired from the structural mode analysis via the finite element method (FEM) [32] or experiment or both. From the structural mode analysis, one can get the transfer function from the force u_2 generated by pulse thrusters to the additive attitude e, which is usually high-order, in the form of

$$\frac{e(s)}{u_2(s)} = \frac{b_0 s^m + b_1 s^{m-1} + \cdots + b_{m-1}s + b_m}{s^m + a_1 s^{m-1} + \cdots + a_{m-1}s + a_m}, \quad m \geqslant 1 \tag{6}$$

where $a_1, a_2, \cdots, a_m$ and $b_0, b_1, \cdots, b_m$ are non-negative constants.

In order to describe system (6) in state space, we choose state variables as

$$\begin{cases} x_3 = e - b_0 u_2 \\ x_4 = \dot{x}_3 - h_1 u_2 \\ \quad \vdots \\ x_{m+2} = \dot{x}_{m+1} - h_m u_2 \end{cases} \tag{7}$$

where

$$\begin{cases} h_1 = b_1 - a_1 b_0 \\ h_2 = (b_2 - a_2 b_0) - a_1 h_1 \\ h_3 = (b_3 - a_3 b_0) - a_2 h_1 - a_1 h_2 \\ \quad \vdots \\ h_m = (b_m - a_m b_0) - a_{m-1} h_1 - \\ a_{m-2} h_2 - \cdots - a_2 h_{m-2} - a_1 h_{m-1} \end{cases}. \tag{8}$$

Letting $n=m+2$, the transfer function (6) can be then converted to

$$\begin{cases} \dot{x}_3 = x_4 + h_1 u_2 \\ \dot{x}_4 = x_5 + h_2 u_2 \\ \quad\vdots \\ \dot{x}_n = -a_{n-2}x_3 - a_{n-3}x_4 - \cdots - a_1 x_n + h_{n-2}u_2 \\ e = x_3 + b_0 u_2 \end{cases}, \tag{9}$$

or in the matrix form:

$$\begin{cases} \dot{\boldsymbol{x}}_2 = \boldsymbol{A}_2\boldsymbol{x}_2 + \boldsymbol{B}_2\boldsymbol{u}_2 \\ \boldsymbol{e} = \boldsymbol{C}_2\boldsymbol{x}_2 + \boldsymbol{D}_2\boldsymbol{u}_2 \end{cases} \tag{10}$$

where

$$\begin{gathered} \boldsymbol{x}_2 = [\ x_3 \quad x_4 \quad \cdots \quad x_n\ ]^{\mathrm{T}}, \\ \boldsymbol{A}_2 = \begin{bmatrix} 0 & 1 & 0 & \cdots & 0 \\ 0 & 0 & 1 & \cdots & 0 \\ \vdots & \vdots & \vdots & \ddots & \vdots \\ 0 & 0 & 0 & \cdots & 1 \\ -a_{n-2} & -a_{n-3} & -a_{n-4} & \cdots & -a_1 \end{bmatrix}, \\ \boldsymbol{B}_2 = [\ h_1 \quad h_2 \quad \cdots \quad h_{n-2}\ ]^{\mathrm{T}}, \\ \boldsymbol{C}_2 = [\ 1 \quad 0 \quad \cdots \quad 0\ ], \boldsymbol{D}_2 = b_0. \end{gathered} \tag{11}$$

The additive attitude error in the IMU can also be calculated by a model similar to (6) with different parameters. The rigid body attitude can thus be corrected. Denote z as the LOS angle decoupled by the corrected attitude measurement. Assume that the error in LOS angle equals the additive attitude, i.e.,

$$z = x_1 + e. \tag{12}$$

Choose $\boldsymbol{x} = \begin{bmatrix} \boldsymbol{x}_1^{\mathrm{T}} & \boldsymbol{x}_2^{\mathrm{T}} \end{bmatrix}^{\mathrm{T}}$ as the augmented state vector. By combining (4), (10) and (12), one can get the state equation and the measurement equation of the augmented state system, i.e.,

$$\begin{cases} \dot{\boldsymbol{x}} = \boldsymbol{A}(t)\boldsymbol{x} + \boldsymbol{B}(t)\boldsymbol{u} \\ z = \boldsymbol{C}\boldsymbol{x} + \boldsymbol{D}\boldsymbol{u} \end{cases} \tag{13}$$

where

$$\begin{gathered} \boldsymbol{A}(t) = \begin{bmatrix} \boldsymbol{A}_1(t) & \\ & \boldsymbol{A}_2 \end{bmatrix}, \boldsymbol{B}(t) = \begin{bmatrix} \boldsymbol{B}_1(t) & \\ & \boldsymbol{B}_2 \end{bmatrix}, \\ \boldsymbol{C} = [\ \boldsymbol{C}_1 \quad \boldsymbol{C}_2\ ], \boldsymbol{C}_1 = [\ 1 \quad 0\ ], \boldsymbol{D} = [\ \boldsymbol{0} \quad \boldsymbol{D}_2\ ], \\ \boldsymbol{u} = [\ u_1 \quad u_2\ ]^{\mathrm{T}}, \boldsymbol{z} = z, \end{gathered} \tag{14}$$

which is a linear time-variant system.

3. Observability analysis

In control theory, observability is a measure of how well internal states of a system can be inferred from the knowledge of its external outputs. Informally, this means that one can determine the behavior of the entire system only from the system's outputs. If the system equation satisfies the observability condition, the estimate of the Kalman filter will converge to track the system perfectly as time progressing, even if we start with an arbitrary state estimate. The observability analysis for system (13) in this section is based on the observability rank condition for linear time-variant systems shown in the lemma below.

Lemma 1 [33] Given a linear time-variant system

$$\begin{cases} \dot{\boldsymbol{x}} = \boldsymbol{A}(t)\boldsymbol{x} + \boldsymbol{B}(t)\boldsymbol{u} \\ \boldsymbol{z} = \boldsymbol{C}(t)\boldsymbol{x} + \boldsymbol{D}(t)\boldsymbol{u} \end{cases} \tag{15}$$

where $\boldsymbol{x} \in \mathbf{R}^n, \boldsymbol{u} \in \mathbf{R}^l, \boldsymbol{z} \in \mathbf{R}^p$. Let

$$\begin{cases} \boldsymbol{O}_0(t) = \boldsymbol{C}(t) \\ \boldsymbol{O}_{i+1}(t) = \boldsymbol{O}_i(t)\boldsymbol{A}(t) + \dot{\boldsymbol{O}}_i(t), \ \ i = 0, 1, \cdots, n-2 \end{cases}. \tag{16}$$

The system is observable in the interval $[t_0, t_f]$ if the observability matrix

$$\boldsymbol{O}(t) = \begin{bmatrix} \boldsymbol{O}_0(t) \\ \boldsymbol{O}_1(t) \\ \vdots \\ \boldsymbol{O}_{n-1}(t) \end{bmatrix} \tag{17}$$

satisfies

$$\operatorname{rank} \boldsymbol{O}(t_f) = n. \tag{18}$$

The observability of the model (13) is described in the theorem as follows.

Theorem 1 The system model (13) is observable during the nearly whole terminal guidance phase.

Proof Apply the lemma in system model (13) described in this paper, one can get

$$\begin{cases} \boldsymbol{O}_0 = [\ 1 \quad 0 \quad 1 \quad 0 \quad \cdots \quad 0\ ] \\ \boldsymbol{O}_1 = \boldsymbol{O}_0 A(t) + \dot{\boldsymbol{O}}_0 = [\ 0 \quad 1 \quad 0 \quad 1 \quad \cdots \quad 0\ ] \\ \boldsymbol{O}_2 = \boldsymbol{O}_1 A(t) + \dot{\boldsymbol{O}}_1 = [\ 0 \quad p_1 \quad 0 \quad 0 \quad \cdots \quad 0\ ] \\ \boldsymbol{O}_3 = \boldsymbol{O}_2 A(t) + \dot{\boldsymbol{O}}_2 = [\ 0 \quad p_2 \quad 0 \quad 0 \quad \cdots \quad 0\ ] \\ \quad\vdots \\ \boldsymbol{O}_{n-2} = \boldsymbol{O}_{n-3} A(t) + \dot{\boldsymbol{O}}_{n-3} = \\ [\ 0 \quad p_{n-3} \quad -a_{n-2} \quad -a_{n-3} \quad \cdots \quad -a_1\ ] \\ \boldsymbol{O}_{n-1} = \boldsymbol{O}_{n-2} A(t) + \dot{\boldsymbol{O}}_{n-2} = \\ [\ 0 \quad p_{n-2} \quad a_1 a_{n-2} \quad a_1 a_{n-3} - a_{n-2} \quad \cdots \quad a_1^2 - a_2\ ] \end{cases} \tag{19}$$

where

$$\begin{cases} p_1 = -\dfrac{2\dot{r}}{r} \\ p_{j+1} = -\dfrac{2\dot{r}+j}{r} p_j, \ \ j = 1, 2, \cdots, n-3. \end{cases} \tag{20}$$

Thus, the observability matrix is composed by $\boldsymbol{O}_0$, $\boldsymbol{O}_1, \cdots, \boldsymbol{O}_{n-1}$ in the following form:

$$\boldsymbol{O}=\begin{bmatrix} 1 & 0 & 1 & 0 & \cdots & 0 \\ 0 & 1 & 0 & 1 & \cdots & 0 \\ 0 & p_1 & \vdots & \vdots & \ddots & \vdots \\ 0 & p_2 & 0 & 0 & \cdots & 1 \\ \vdots & \vdots & -a_{n-2} & -a_{n-3} & \cdots & -a_1 \\ 0 & p_{n-2} & a_1a_{n-2} & a_1a_{n-3}-a_{n-2} & \cdots & a_1^2-a_2 \end{bmatrix}. \tag{21}$$

The key to the observability analysis is to determine the rank of $\boldsymbol{O}$, which is quite complicated in most cases. Notice that there exists an $n-2$ dimensional identity in the top-right corner of the matrix, meaning that $\boldsymbol{O}_0$, $\boldsymbol{O}_1,\cdots,\boldsymbol{O}_{n-3}$ are linearly independent. Besides, $\boldsymbol{O}_{n-2}$ cannot be expressed by the linear combination of $\boldsymbol{O}_0$, $\boldsymbol{O}_1,\cdots,\boldsymbol{O}_{n-3}$. Therefore, the observability matrix does not have full rank if and only if $\boldsymbol{O}_{n-1}$ can be expressed by the linear combination of $\boldsymbol{O}_0,\boldsymbol{O}_1,\cdots,\boldsymbol{O}_{n-2}$. What should the linear expression be like? Notice that only $\boldsymbol{O}_0$ has a nonzero element in its first component, so the coefficient before $\boldsymbol{O}_0$ should be zero. By observing the third, the fourth until the last component of the bases sequentially one can determine all coefficients. The only possible linear expression can be as

$$\boldsymbol{O}_{n-1}=-a_1\boldsymbol{O}_{n-2}-a_2\boldsymbol{O}_{n-3}-\cdots-a_{n-2}\boldsymbol{O}_1. \tag{22}$$

Observe the second component of each item above, one can get

$$p_{n-2}+a_1p_{n-3}+a_2p_{n-4}+\cdots+a_{n-3}p_1+a_{n-2}=0. \tag{23}$$

Considering (20), the solution to (23) is no more than m separate values for r. During the terminal guidance phase, r varies continuously and tends to zero. There must exists a t_1 near to and less than t_f where (23) does not hold and therefore rank $\boldsymbol{O}(t_1)=n$. Thus, the system is observable in the interval $[t_0,t_1]$.

Specially, when $m=1$, the condition turns to be

$$a_1-\frac{2\dot{r}}{r}=0, \tag{24}$$

which almost impossibly holds in practice because r is a time-variant variable. Even if it holds at the final time t_f unfortunately, we can tell that the system is observable in the interval $[t_0,t_1]$ where t_1 is quite near to and less than t_f.

4. Filter design

4.1 Continuous-discrete augmented state Kalman filter

The Kalman filter is an efficient recursive filter that estimates the internal state of a linear dynamic system from a series of noisy measurements. It is used in a wide range of engineering and econometric applications from radar and computer vision to estimation of structural macroeconomic models [34].

The Kalman filter algorithm can be divided into two phases: a prediction phase and an update phase [35]. In the prediction phase, the state estimate from the previous time instance to produce an estimate of the state at the current time instance via the dynamical model. In the update phase, the current prediction is combined with current observation information to refine the state estimate.

In engineering applications, the Kalman filter is usually performed in discrete form. However, since the system model (13) is time-variant and high-order, the exact discretization of the continuous-time dynamical model is difficult. On the other hand, the measurements are obtained at discrete times. Therefore, the continuous-discrete version of Kalman filter will be applied for the problem.

The system model (13) can be easily converted to the model assumed in continuous discrete Kalman filter by adding corresponding noises as

$$\begin{cases} \dot{\boldsymbol{x}}=\boldsymbol{A}(t)\boldsymbol{x}+\boldsymbol{B}(t)\boldsymbol{u}+\boldsymbol{\omega} \\ \boldsymbol{z}_k=\boldsymbol{C}\boldsymbol{x}_k+\boldsymbol{D}\boldsymbol{u}_k+\boldsymbol{\nu}_k,\ k\geqslant 1 \end{cases} \tag{25}$$

where $\boldsymbol{x}_k$, $\boldsymbol{u}_k$ and $\boldsymbol{\nu}_k$ denote $\boldsymbol{x}(t_k)$, $\boldsymbol{u}(t_k)$ and $\boldsymbol{\nu}(t_k)$, respectively; $\boldsymbol{A}(t)$, $\boldsymbol{B}(t)$, $\boldsymbol{C}$ and $\boldsymbol{D}$ are the same as in (13); $\boldsymbol{\omega}(t)$ is the process noise which is assumed to be zero mean Gaussian white noise with spectral density matrix $\boldsymbol{Q}\triangleq\operatorname{diag}(\boldsymbol{Q}_1,\boldsymbol{Q}_2)$ where $\boldsymbol{Q}_1$ corresponds to the original state $\boldsymbol{x}_1$ and $\boldsymbol{Q}_2$ corresponds to the bias state $\boldsymbol{x}_2$; $\boldsymbol{\nu}_k$ is the observation noise which is assumed to be zero mean Gaussian white noise with covariance R. The initial state and the noise vectors at each step are all assumed to be mutually independent. The so-called continuous-discrete augmented state Kalman filter algorithm is just the continuous-discrete Kalman filter algorithm applied in the augmented state system (25), which is shown in detail as follows.

Algorithm 1 Continuous-discrete augmented state Kalman filter (CD-ASKF)

For the augmented state system model (25), given the estimated mean $\hat{\boldsymbol{x}}_{k-1|k-1}$ and covariance $\boldsymbol{P}_{k-1|k-1}$ at time instant t_{k-1}, the estimated mean $\hat{\boldsymbol{x}}_{k|k}$ and covariance $\boldsymbol{P}_{k|k}$ at time instance t_k is obtained by following steps.

Step 1 Prediction

Integrate the differential equations

$$\dot{\hat{\boldsymbol{x}}}=\boldsymbol{A}(t)\hat{\boldsymbol{x}}+\boldsymbol{B}(t)\boldsymbol{u}, \tag{26}$$

$$\dot{\boldsymbol{P}}=\boldsymbol{A}(t)\boldsymbol{P}+\boldsymbol{P}\boldsymbol{A}(t)^{\mathrm{T}}+\boldsymbol{Q}, \tag{27}$$

from the initial conditions $\hat{\boldsymbol{x}}(t_{k-1})=\hat{\boldsymbol{x}}_{k-1|k-1}$ and $\boldsymbol{P}(t_{k-1})=\boldsymbol{P}_{k-1|k-1}$ to time instance t_k. The predicted mean and cova-

riance are given as $\hat{\boldsymbol{x}}_{k|k-1}=\hat{\boldsymbol{x}}(t_k)$ and $\boldsymbol{P}_{k|k-1}=\boldsymbol{P}(t_k)$. The integration can be computed by numerical integration methods such as Runge-Kutta fourth-order method.

Step 2 Update

The update step is the same as the discrete-time Kalman filter, given by

$$\boldsymbol{K}_k=\boldsymbol{P}_{k|k-1}\boldsymbol{C}^{\mathrm{T}}(\boldsymbol{C}\boldsymbol{P}_{k|k-1}\boldsymbol{C}^{\mathrm{T}}+\boldsymbol{R})^{-1}, \tag{28}$$

$$\hat{\boldsymbol{x}}_{k|k}=\hat{\boldsymbol{x}}_{k|k-1}+\boldsymbol{K}_k[\boldsymbol{z}_k-(\boldsymbol{C}\hat{\boldsymbol{x}}_{k|k-1}+\boldsymbol{D}\boldsymbol{u}_k)], \tag{29}$$

$$\boldsymbol{P}_{k|k}=(\boldsymbol{I}-\boldsymbol{K}_k\boldsymbol{C})\boldsymbol{P}_{k|k-1}. \tag{30}$$

The selection of the process noise spectral density matrix $\boldsymbol{Q}$ depends on the uncertainty of the dynamical model. In the process of the terminal guidance of KKV, it is quite small.

The selection of the observation noise covariance $\boldsymbol{R}_k$ depends on the accuracy of the seeker.

The initial state estimate can be chosen as the first measurement of the seeker. The initial state estimate of the additive attitude e can be chosen as 0.

4.2 Continuous-discrete two-stage Kalman filter (CD-TSKF)

The ASKF is intuitive, but causes higher computational cost and round-off error. TSKF is a method of decoupling the augmented filter into two parallel and lower-order filters. The difficulty in decoupling the CD-ASKF (26)−(30) is that the covariance of augmented state is not block diagonal, which means that the original state $\boldsymbol{x}_1$ and the bias state $\boldsymbol{x}_2$ are correlated. To solve the problem, define a bias free state

$$\tilde{\boldsymbol{x}}_1=\boldsymbol{x}_1-\boldsymbol{V}\boldsymbol{x}_2, \tag{31}$$

which is uncorrelated with $\boldsymbol{x}_2$. The blending matrix $\boldsymbol{V}$ is defined by [25]

$$\boldsymbol{V}=\mathrm{cov}(\boldsymbol{x}_1,\boldsymbol{x}_2)[\mathrm{cov}(\boldsymbol{x}_2)]^{-1}. \tag{32}$$

The two decoupled filters, called as bias free filter and bias filter, can be run in parallel way (with some connection) to give the estimates of $\tilde{\boldsymbol{x}}_1$ and $\boldsymbol{x}_2$, respectively. The estimate of $\boldsymbol{x}_1$ is obtained via the mixture of the two filters' outputs.

Algorithm 2 CD-TSKF

For the augmented state system model (25), the CD-TSKF consists of the following decoupled filters.

(i) Bias free filter

Given the blending matrix $\boldsymbol{V}_{k-1|k-1}$, the estimated mean $\hat{\tilde{\boldsymbol{x}}}_{1,k-1|k-1}$ and covariance $\tilde{\boldsymbol{P}}_{1,k-1|k-1}$ at time instant t_{k-1}, the blending matrix $\boldsymbol{V}_{k|k}$ and the estimated mean $\hat{\tilde{\boldsymbol{x}}}_{1,k|k}$ and covariance $\tilde{\boldsymbol{P}}_{1,k|k}$ at time instance t_k are obtained by following steps.

Step 1 Prediction

Given the predicted mean $\hat{\boldsymbol{x}}_2$ and covariance $\boldsymbol{P}_2$ at time instance t_k from the bias filter, integrate the differential equations

$$\dot{\boldsymbol{V}}=\boldsymbol{A}_1(t)\boldsymbol{V}-\boldsymbol{V}\boldsymbol{A}_2-\boldsymbol{V}\boldsymbol{Q}_2\boldsymbol{P}_2^{-1}, \tag{33}$$

$$\dot{\hat{\tilde{\boldsymbol{x}}}}_1=\boldsymbol{A}_1(t)\hat{\tilde{\boldsymbol{x}}}_1+\boldsymbol{B}_1(t)u_1+\boldsymbol{V}\boldsymbol{Q}_2\boldsymbol{P}_2^{-1}\hat{\boldsymbol{x}}_2-\boldsymbol{V}\boldsymbol{B}_2u_2, \tag{34}$$

$$\dot{\tilde{\boldsymbol{P}}}_1=\boldsymbol{A}_1(t)\tilde{\boldsymbol{P}}_1+\tilde{\boldsymbol{P}}_1\boldsymbol{A}_1^{\mathrm{T}}(t)+\boldsymbol{Q}_1+\boldsymbol{V}\boldsymbol{Q}_2\boldsymbol{V}^{\mathrm{T}}, \tag{35}$$

from the initial conditions $\boldsymbol{V}(t_{k-1})=\boldsymbol{V}_{k-1|k-1}$, $\hat{\tilde{\boldsymbol{x}}}_1(t_{k-1})=\hat{\tilde{\boldsymbol{x}}}_{1,k-1|k-1}$ and $\tilde{\boldsymbol{P}}_1(t_{k-1})=\tilde{\boldsymbol{P}}_{1,k-1|k-1}$ to time instance t_k. The predicted blending matrix, mean and covariance are given as $\boldsymbol{V}_{k|k-1}=\boldsymbol{V}(t_k)$, $\hat{\tilde{\boldsymbol{x}}}_{1,k|k-1}=\hat{\tilde{\boldsymbol{x}}}_1(t_k)$ and $\tilde{\boldsymbol{P}}_{1,k|k-1}=\tilde{\boldsymbol{P}}_1(t_k)$. The integration can be computed by numerical integration methods such as Runge-Kutta fourth-order method.

Step 2 Update

The updated blending matrix, mean and covariance are given by

$$\boldsymbol{K}_{1,k}=\tilde{\boldsymbol{P}}_{1,k|k-1}\boldsymbol{C}_1^{\mathrm{T}}(\boldsymbol{C}_1\tilde{\boldsymbol{P}}_{1,k|k-1}\boldsymbol{C}_1^{\mathrm{T}}+\boldsymbol{R})^{-1}, \tag{36}$$

$$\boldsymbol{S}_k=\boldsymbol{C}_1\boldsymbol{V}_{k|k-1}+\boldsymbol{C}_2, \tag{37}$$

$$\boldsymbol{V}_{k|k}=\boldsymbol{V}_{k|k-1}-\boldsymbol{K}_{1,k}\boldsymbol{S}_k, \tag{38}$$

$$\hat{\tilde{\boldsymbol{x}}}_{1,k|k}=\hat{\tilde{\boldsymbol{x}}}_{1,k|k-1}+\boldsymbol{K}_{1,k}(\boldsymbol{z}_k-\boldsymbol{C}_1\hat{\tilde{\boldsymbol{x}}}_{1,k|k-1}-\boldsymbol{D}_2u_2), \tag{39}$$

$$\tilde{\boldsymbol{P}}_{1,k|k}=(\boldsymbol{I}-\boldsymbol{K}_{1,k}\boldsymbol{C}_1)\tilde{\boldsymbol{P}}_{1,k|k-1}. \tag{40}$$

(ii) Bias filter

Given the estimated mean $\hat{\boldsymbol{x}}_{2,k-1|k-1}$ and covariance $\boldsymbol{P}_{2,k-1|k-1}$ at time instant t_{k-1}, the estimated mean $\hat{\boldsymbol{x}}_{2,k|k}$ and covariance $\boldsymbol{P}_{2,k|k}$ at time instance t_k are obtained by following steps.

Step 1 Prediction

Integrate the differential equations

$$\dot{\hat{\boldsymbol{x}}}_2=\boldsymbol{A}_2\hat{\boldsymbol{x}}_2+\boldsymbol{B}_2u_2, \tag{41}$$

$$\dot{\boldsymbol{P}}_2=\boldsymbol{A}_2\boldsymbol{P}_2+\boldsymbol{P}_2\boldsymbol{A}_2^{\mathrm{T}}+\boldsymbol{Q}_2, \tag{42}$$

from the initial conditions $\hat{\boldsymbol{x}}_2(t_{k-1})=\hat{\boldsymbol{x}}_{2,k-1|k-1}$ and $\boldsymbol{P}_2(t_{k-1})=\boldsymbol{P}_{2,k-1|k-1}$ to time instance t_k. The predicted mean and covariance are given as $\hat{\boldsymbol{x}}_{2,k|k-1}=\hat{\boldsymbol{x}}_2(t_k)$ and $\boldsymbol{P}_{2,k|k-1}=\boldsymbol{P}_2(t_k)$. The integration can be computed by numerical integration methods such as Runge-Kutta fourth-order method.

Step 2 Update

Given $\boldsymbol{S}_k$, the predicted mean $\hat{\tilde{\boldsymbol{x}}}_{1,k|k-1}$ and covariance $\tilde{\boldsymbol{P}}_{1,k|k-1}$ from the bias free filter, the updated mean and covariance are given by

$$\boldsymbol{K}_{2,k}=\boldsymbol{P}_{2,k|k-1}\boldsymbol{S}_k^{\mathrm{T}}(\boldsymbol{C}_1\tilde{\boldsymbol{P}}_{1,k|k-1}\boldsymbol{C}_1^{\mathrm{T}}+\boldsymbol{S}_k\boldsymbol{P}_{2,k|k-1}\boldsymbol{S}_k^{\mathrm{T}}+\boldsymbol{R})^{-1}, \tag{43}$$

$$\hat{\boldsymbol{x}}_{2,k|k}=\hat{\boldsymbol{x}}_{2,k|k-1}+\boldsymbol{K}_{2,k}(\boldsymbol{z}_k-\boldsymbol{C}_1\hat{\tilde{\boldsymbol{x}}}_{1,k|k-1}-\boldsymbol{S}_k\hat{\boldsymbol{x}}_{2,k|k-1}-\boldsymbol{D}_2\boldsymbol{u}_2), \quad (44)$$

$$\boldsymbol{P}_{2,k|k}=(\boldsymbol{I}-\boldsymbol{K}_{2,k}\boldsymbol{S}_k)\boldsymbol{P}_{2,k|k-1}. \quad (45)$$

(iii) Mixing

The estimate of original state is given by

$$\begin{cases}\hat{\boldsymbol{x}}_{1,k|k}=\hat{\tilde{\boldsymbol{x}}}_{1,k|k}+\boldsymbol{V}_{k|k}\hat{\boldsymbol{x}}_{2,k|k}\\ \boldsymbol{P}_{1,k|k}=\tilde{\boldsymbol{P}}_{1,k|k}+\boldsymbol{V}_{k|k}\boldsymbol{P}_{2,k|k}\boldsymbol{V}_{k|k}^{\mathrm{T}}\end{cases}. \quad (46)$$

The selection of initial mean $\hat{\boldsymbol{x}}_{0|0}$, covariance $\boldsymbol{P}_{0|0}$, spectral density matrix $\boldsymbol{Q}$ of process noise and covariance $\boldsymbol{R}_k$ are the same as CD-ASKF. Since $\boldsymbol{P}_{0|0}$ is often chosen as diagonal, one can set $\hat{\tilde{\boldsymbol{x}}}_{1,0|0}=\hat{\boldsymbol{x}}_{1,0|0}$, $\tilde{\boldsymbol{P}}_{1,0|0}=\boldsymbol{P}_{1,0|0}$ and $\boldsymbol{V}_{0|0}=\boldsymbol{0}$.

Theorem 2 The CD-TSKF (Algorithm 2) is equivalent to the CD-ASKF (Algorithm 1).

Proof From (31), the mean and covariance of $\boldsymbol{x}_1$ are given by

$$\begin{cases}\hat{\boldsymbol{x}}_1=\hat{\tilde{\boldsymbol{x}}}_1+\boldsymbol{V}\hat{\boldsymbol{x}}_2\\ \boldsymbol{P}_1=\tilde{\boldsymbol{P}}_1+\boldsymbol{V}\boldsymbol{P}_2\boldsymbol{V}^{\mathrm{T}}\end{cases}. \quad (47)$$

The mean and covariance of the augmented state are

$$\hat{\boldsymbol{x}}=\begin{bmatrix}\hat{\tilde{\boldsymbol{x}}}_1+\boldsymbol{V}\hat{\boldsymbol{x}}_2\\ \hat{\boldsymbol{x}}_2\end{bmatrix}, \quad (48)$$

$$\boldsymbol{P}=\begin{bmatrix}\mathrm{cov}(\boldsymbol{x}_1) & \mathrm{cov}(\boldsymbol{x}_1,\boldsymbol{x}_2)\\ \mathrm{cov}(\boldsymbol{x}_2,\boldsymbol{x}_1) & \mathrm{cov}(\boldsymbol{x}_2)\end{bmatrix}=\begin{bmatrix}\tilde{\boldsymbol{P}}_1+\boldsymbol{V}\boldsymbol{P}_2\boldsymbol{V}^{\mathrm{T}} & \boldsymbol{V}\boldsymbol{P}_2\\ \boldsymbol{P}_2\boldsymbol{V}^{\mathrm{T}} & \boldsymbol{P}_2\end{bmatrix}. \quad (49)$$

Here we use $\boldsymbol{A}_1$, $\boldsymbol{B}_1$ instead of $\boldsymbol{A}_1(t)$, $\boldsymbol{B}_1(t)$ for simplify. By using the equations in Algorithm 2 and a few algebra tricks, one can see that

$$\dot{\hat{\boldsymbol{x}}}=\begin{bmatrix}\dot{\hat{\tilde{\boldsymbol{x}}}}_1+\dot{\boldsymbol{V}}\hat{\boldsymbol{x}}_2+\boldsymbol{V}\dot{\hat{\boldsymbol{x}}}_2\\ \dot{\hat{\boldsymbol{x}}}_2\end{bmatrix}=\begin{bmatrix}\left(\boldsymbol{A}_1\hat{\tilde{\boldsymbol{x}}}_1+\boldsymbol{B}_1\boldsymbol{u}_1+\boldsymbol{V}\boldsymbol{Q}_2\boldsymbol{P}_2^{-1}\hat{\boldsymbol{x}}_2-\boldsymbol{V}\boldsymbol{B}_2\boldsymbol{u}_2\right)+(\boldsymbol{A}_1\boldsymbol{V}-\boldsymbol{V}\boldsymbol{A}_2-\boldsymbol{V}\boldsymbol{Q}_2\boldsymbol{P}_2^{-1})\hat{\boldsymbol{x}}_2+\boldsymbol{V}(\boldsymbol{A}_2\hat{\boldsymbol{x}}_2+\boldsymbol{B}_2\boldsymbol{u}_2)\\ \boldsymbol{A}_2\hat{\boldsymbol{x}}_2+\boldsymbol{B}_2\boldsymbol{u}_2\end{bmatrix}=$$
$$\begin{bmatrix}\boldsymbol{A}_1\left(\hat{\tilde{\boldsymbol{x}}}_1+\boldsymbol{V}\hat{\boldsymbol{x}}_2\right)+\boldsymbol{B}_1\boldsymbol{u}_1\\ \boldsymbol{A}_2\hat{\boldsymbol{x}}_2+\boldsymbol{B}_2\boldsymbol{u}_2\end{bmatrix}=\begin{bmatrix}\boldsymbol{A}_1& \\ & \boldsymbol{A}_2\end{bmatrix}\begin{bmatrix}\hat{\tilde{\boldsymbol{x}}}_1+\boldsymbol{V}\hat{\boldsymbol{x}}_2\\ \hat{\boldsymbol{x}}_2\end{bmatrix}+\begin{bmatrix}\boldsymbol{B}_1 & \\ & \boldsymbol{B}_2\end{bmatrix}\boldsymbol{u}=\boldsymbol{A}(t)\hat{\boldsymbol{x}}+\boldsymbol{B}(t)\boldsymbol{u}, \quad (50)$$

$$\dot{\boldsymbol{P}}=\begin{bmatrix}\dot{\tilde{\boldsymbol{P}}}_1+\dot{\boldsymbol{V}}\boldsymbol{P}_2\boldsymbol{V}^{\mathrm{T}}+\boldsymbol{V}\dot{\boldsymbol{P}}_2\boldsymbol{V}^{\mathrm{T}}+\boldsymbol{V}\boldsymbol{P}_2\dot{\boldsymbol{V}}^{\mathrm{T}} & \dot{\boldsymbol{V}}\boldsymbol{P}_2+\boldsymbol{V}\dot{\boldsymbol{P}}_2\\ \dot{\boldsymbol{P}}_2\boldsymbol{V}^{\mathrm{T}}+\boldsymbol{P}_2\dot{\boldsymbol{V}}^{\mathrm{T}} & \dot{\boldsymbol{P}}_2\end{bmatrix}=$$
$$\begin{bmatrix}(\boldsymbol{A}_1\tilde{\boldsymbol{P}}_1+\tilde{\boldsymbol{P}}_1\boldsymbol{A}_1^{\mathrm{T}}+\boldsymbol{Q}_1+\boldsymbol{V}\boldsymbol{Q}_2\boldsymbol{V}^{\mathrm{T}})+(\boldsymbol{A}_1\boldsymbol{V}-\boldsymbol{V}\boldsymbol{A}_2-\boldsymbol{V}\boldsymbol{Q}_2\boldsymbol{P}_2^{-1})\boldsymbol{P}_2\boldsymbol{V}^{\mathrm{T}}+ & (\boldsymbol{A}_1\boldsymbol{V}-\boldsymbol{V}\boldsymbol{A}_2-\boldsymbol{V}\boldsymbol{Q}_2\boldsymbol{P}_2^{-1})\boldsymbol{P}_2+\\ \boldsymbol{V}(\boldsymbol{A}_2\boldsymbol{P}_2+\boldsymbol{P}_2\boldsymbol{A}_2^{\mathrm{T}}+\boldsymbol{Q}_2)\boldsymbol{V}^{\mathrm{T}}+\boldsymbol{V}\boldsymbol{P}_2(\boldsymbol{A}_1\boldsymbol{V}-\boldsymbol{V}\boldsymbol{A}_2-\boldsymbol{V}\boldsymbol{Q}_2\boldsymbol{P}_2^{-1})^{\mathrm{T}} & \boldsymbol{V}(\boldsymbol{A}_2\boldsymbol{P}_2+\boldsymbol{P}_2\boldsymbol{A}_2^{\mathrm{T}}+\boldsymbol{Q}_2)\\ (\boldsymbol{A}_2\boldsymbol{P}_2+\boldsymbol{P}_2\boldsymbol{A}_2^{\mathrm{T}}+\boldsymbol{Q}_2)\boldsymbol{V}^{\mathrm{T}}+\boldsymbol{P}_2(\boldsymbol{A}_1\boldsymbol{V}-\boldsymbol{V}\boldsymbol{A}_2-\boldsymbol{V}\boldsymbol{Q}_2\boldsymbol{P}_2^{-1})^{\mathrm{T}} & \boldsymbol{A}_2\boldsymbol{P}_2+\boldsymbol{P}_2\boldsymbol{A}_2^{\mathrm{T}}+\boldsymbol{Q}_2\end{bmatrix}=$$
$$\begin{bmatrix}\boldsymbol{A}_1 & \\ & \boldsymbol{A}_2\end{bmatrix}\begin{bmatrix}\tilde{\boldsymbol{P}}_1+\boldsymbol{V}\boldsymbol{P}_2\boldsymbol{V}^{\mathrm{T}} & \boldsymbol{V}\boldsymbol{P}_2\\ \boldsymbol{P}_2\boldsymbol{V}^{\mathrm{T}} & \boldsymbol{P}_2\end{bmatrix}+\begin{bmatrix}\tilde{\boldsymbol{P}}_1+\boldsymbol{V}\boldsymbol{P}_2\boldsymbol{V}^{\mathrm{T}} & \boldsymbol{V}\boldsymbol{P}_2\\ \boldsymbol{P}_2\boldsymbol{V}^{\mathrm{T}} & \boldsymbol{P}_2\end{bmatrix}\begin{bmatrix}\boldsymbol{A}_1 & \\ & \boldsymbol{A}_2\end{bmatrix}^{\mathrm{T}}+\begin{bmatrix}\boldsymbol{Q}_1 & \\ & \boldsymbol{Q}_2\end{bmatrix}=$$
$$\boldsymbol{A}(t)\boldsymbol{P}+\boldsymbol{P}\boldsymbol{A}^{\mathrm{T}}(t)+\boldsymbol{Q}, \quad (51)$$

$$\boldsymbol{K}_k=\begin{bmatrix}\tilde{\boldsymbol{P}}_{1,k|k-1}+\boldsymbol{V}_{k|k-1}\boldsymbol{P}_{2,k|k-1}\boldsymbol{V}_{k|k-1}^{\mathrm{T}} & \boldsymbol{V}_{k|k-1}\boldsymbol{P}_{2,k|k-1}\\ \boldsymbol{P}_{2,k|k-1}\boldsymbol{V}_{k|k-1}^{\mathrm{T}} & \boldsymbol{P}_{2,k|k-1}\end{bmatrix}[\ \boldsymbol{C}_1\quad \boldsymbol{C}_2\ ]^{\mathrm{T}}\cdot$$
$$\left([\ \boldsymbol{C}_1\quad \boldsymbol{C}_2\ ]\begin{bmatrix}\tilde{\boldsymbol{P}}_{1,k|k-1}+\boldsymbol{V}_{k|k-1}\boldsymbol{P}_{2,k|k-1}\boldsymbol{V}_{k|k-1}^{\mathrm{T}} & \boldsymbol{V}_{k|k-1}\boldsymbol{P}_{2,k|k-1}\\ \boldsymbol{P}_{2,k|k-1}\boldsymbol{V}_{k|k-1}^{\mathrm{T}} & \boldsymbol{P}_{2,k|k-1}\end{bmatrix}[\ \boldsymbol{C}_1\quad \boldsymbol{C}_2\ ]^{\mathrm{T}}+\boldsymbol{R}\right)^{-1}=$$
$$\begin{bmatrix}\tilde{\boldsymbol{P}}_{1,k|k-1}\boldsymbol{C}_1^{\mathrm{T}}+\boldsymbol{V}_{k|k-1}\boldsymbol{P}_{2,k|k-1}\boldsymbol{S}_k^{\mathrm{T}}\\ \boldsymbol{P}_{2,k|k-1}\boldsymbol{S}_k^{\mathrm{T}}\end{bmatrix}(\boldsymbol{C}_1\tilde{\boldsymbol{P}}_{1,k|k-1}\boldsymbol{C}_1^{\mathrm{T}}+\boldsymbol{S}_k\boldsymbol{P}_{2,k|k-1}\boldsymbol{S}_k^{\mathrm{T}}+\boldsymbol{R})^{-1}=$$
$$\begin{bmatrix}\boldsymbol{K}_{1,k}(\boldsymbol{C}_1\tilde{\boldsymbol{P}}_{1,k|k-1}\boldsymbol{C}_1^{\mathrm{T}}+\boldsymbol{S}_k\boldsymbol{P}_{2,k|k-1}\boldsymbol{S}_k^{\mathrm{T}}+\boldsymbol{R}-\boldsymbol{S}_k\boldsymbol{P}_{2,k|k-1}\boldsymbol{S}_k^{\mathrm{T}})+\boldsymbol{V}_{k|k-1}\boldsymbol{P}_{2,k|k-1}\boldsymbol{S}_k^{\mathrm{T}}\\ \boldsymbol{P}_{2,k|k-1}\boldsymbol{S}_k^{\mathrm{T}}\end{bmatrix}(\boldsymbol{C}_1\tilde{\boldsymbol{P}}_{1,k|k-1}\boldsymbol{C}_1^{\mathrm{T}}+\boldsymbol{S}_k\boldsymbol{P}_{2,k|k-1}\boldsymbol{S}_k^{\mathrm{T}}+\boldsymbol{R})^{-1}=\begin{bmatrix}\boldsymbol{K}_{1,k}+\boldsymbol{V}_{k|k}\boldsymbol{K}_{2,k}\\ \boldsymbol{K}_{2,k}\end{bmatrix}, \quad (52)$$

$$\hat{\boldsymbol{x}}_{k|k}=\begin{bmatrix}\hat{\tilde{\boldsymbol{x}}}_{1,k|k}+\boldsymbol{V}_{k|k}\hat{\boldsymbol{x}}_{2,k|k}\\ \hat{\boldsymbol{x}}_{2,k|k}\end{bmatrix}=\begin{bmatrix}[\hat{\tilde{\boldsymbol{x}}}_{1,k|k-1}+\boldsymbol{K}_{1,k}(\boldsymbol{z}_k-\boldsymbol{C}_1\hat{\tilde{\boldsymbol{x}}}_{1,k|k-1}-\boldsymbol{D}_2\boldsymbol{u}_2)]+(\boldsymbol{V}_{k|k-1}-\boldsymbol{K}_{1,k}\boldsymbol{S}_k)\cdot\\ \left[\hat{\boldsymbol{x}}_{2,k|k-1}+\boldsymbol{K}_{2,k}(\boldsymbol{z}_k-\boldsymbol{C}_1\hat{\tilde{\boldsymbol{x}}}_{1,k|k-1}-\boldsymbol{S}_k\hat{\boldsymbol{x}}_{2,k|k-1}-\boldsymbol{D}_2\boldsymbol{u}_2)\right]\\ \hat{\boldsymbol{x}}_{2,k|k-1}+\boldsymbol{K}_{2,k}[\boldsymbol{z}_k-\boldsymbol{C}_1\hat{\tilde{\boldsymbol{x}}}_{1,k|k-1}-(\boldsymbol{S}_k\hat{\boldsymbol{x}}_{2,k|k-1}+\boldsymbol{D}_2\boldsymbol{u}_2)]\end{bmatrix}=$$
$$\begin{bmatrix}\hat{\tilde{\boldsymbol{x}}}_{1,k|k-1}+\boldsymbol{V}_{k|k-1}\hat{\boldsymbol{x}}_{2,k|k-1}\\ \hat{\boldsymbol{x}}_{2,k|k-1}\end{bmatrix}+\begin{bmatrix}\boldsymbol{K}_{1,k}+\boldsymbol{V}_{k|k}\boldsymbol{K}_{2,k}\\ \boldsymbol{K}_{2,k}\end{bmatrix}\left(\boldsymbol{z}_k-[\boldsymbol{C}_1\quad \boldsymbol{C}_2]\begin{bmatrix}\hat{\tilde{\boldsymbol{x}}}_{1,k|k-1}+\boldsymbol{V}_{k|k-1}\hat{\boldsymbol{x}}_{2,k|k-1}\\ \hat{\boldsymbol{x}}_{2,k|k-1}\end{bmatrix}-[\boldsymbol{0}\quad \boldsymbol{D}_2]\begin{bmatrix}\boldsymbol{u}_1\\ \boldsymbol{u}_2\end{bmatrix}\right)=$$
$$\hat{\boldsymbol{x}}_{k|k-1}+\boldsymbol{K}_k[\boldsymbol{z}_k-(\boldsymbol{C}\hat{\boldsymbol{x}}_{k|k-1}+\boldsymbol{D}\boldsymbol{u})], \quad (53)$$

$$\boldsymbol{P}_{k|k}=\begin{bmatrix}\tilde{\boldsymbol{P}}_{1,k|k}+\boldsymbol{V}_{k|k}\boldsymbol{P}_{2,k|k}\boldsymbol{V}_{k|k}^{\mathrm{T}} & \boldsymbol{V}_{k|k}\boldsymbol{P}_{2,k|k}\\ \boldsymbol{P}_{2,k|k}\boldsymbol{V}_{k|k}^{\mathrm{T}} & \boldsymbol{P}_{2,k|k}\end{bmatrix}=$$
$$\begin{bmatrix}(\boldsymbol{I}-\boldsymbol{K}_{1,k}\boldsymbol{C}_1)\tilde{\boldsymbol{P}}_{1,k|k-1}+(\boldsymbol{V}_{k|k-1}-\boldsymbol{K}_{1,k}\boldsymbol{S}_k)\cdot & \\ (\boldsymbol{I}-\boldsymbol{K}_{2,k}\boldsymbol{S}_k)\boldsymbol{P}_{2,k|k-1}(\boldsymbol{V}_{k|k-1}-\boldsymbol{K}_{1,k}\boldsymbol{S}_k)^{\mathrm{T}} & (\boldsymbol{V}_{k|k-1}-\boldsymbol{K}_{1,k}\boldsymbol{S}_k)(\boldsymbol{I}-\boldsymbol{K}_{2,k}\boldsymbol{S}_k)\boldsymbol{P}_{2,k|k-1}\\ (\boldsymbol{I}-\boldsymbol{K}_{2,k}\boldsymbol{S}_k)\boldsymbol{P}_{2,k|k-1}(\boldsymbol{V}_{k|k-1}-\boldsymbol{K}_{1,k}\boldsymbol{S}_k)^{\mathrm{T}} & (\boldsymbol{I}-\boldsymbol{K}_{2,k}\boldsymbol{S}_k)\boldsymbol{P}_{2,k|k-1}\end{bmatrix}=$$
$$\left(\boldsymbol{I}-\begin{bmatrix}\boldsymbol{K}_{1,k}+\boldsymbol{V}_{k|k}\boldsymbol{K}_{2,k}\\ \boldsymbol{K}_{2,k}\end{bmatrix}\begin{bmatrix}\boldsymbol{C}_1 & \boldsymbol{C}_2\end{bmatrix}\right)\begin{bmatrix}\tilde{\boldsymbol{P}}_{1,k|k-1}+\boldsymbol{V}_{k|k-1}\boldsymbol{P}_{2,k|k-1}\boldsymbol{V}_{k|k-1}^{\mathrm{T}} & \boldsymbol{V}_{k|k-1}\boldsymbol{P}_{2,k|k-1}\\ \boldsymbol{P}_{2,k|k-1}\boldsymbol{V}_{k|k-1}^{\mathrm{T}} & \boldsymbol{P}_{2,k|k-1}\end{bmatrix}=$$
$$(\boldsymbol{I}-\boldsymbol{K}_k\boldsymbol{C})\boldsymbol{P}_{k|k-1}, \tag{54}$$

which are the same as (26)−(30) in Algorithm 1.

5. Numerical simulation

To testify the effect of the designed filter, the numerical simulation is conducted under a typical working condition. The ballistic missile's initial positions in the launch point inertial coordinate system are x_{t_0} = 339.98 km, y_{t_0} = 20.97 km and z_{t_0} = 0 km, respectively. Its initial velocity is V_{t_0} = 1 500 m/s. The KKV's initial point is at the origin of the launch point inertial coordinate system. Its initial velocity is V_{m_0} = 715 m/s. The terminal guidance phase starts at t_0 = 90.183 s. A typical missile-target pursuit curve is shown in Fig. 2.

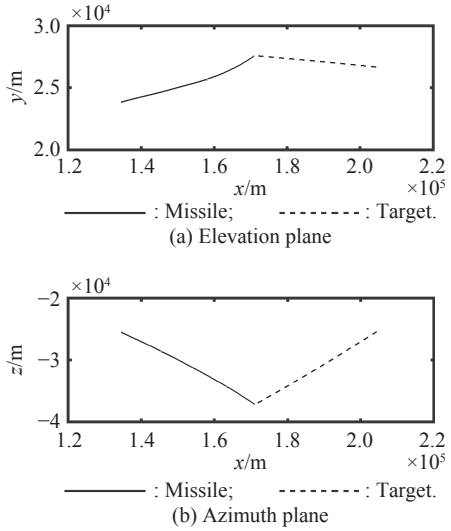

Fig. 2 Typical missile-target pursuit curve

The model of the impact interference of the filter in the simulation is approximated as

$$\frac{e(s)}{u_2(s)}=\frac{2\times10^{-6}s^2+2\times10^{-4}}{s^2+10^2s+10^4}. \tag{55}$$

Simulations are conducted in different cases. In Case 1 the impact interference is ignored in the design of filter, whereas in the latter cases it is considered. In Case 1, the state vector of filter includes LOS angle and LOS rate only. In Case 2, the traditional discrete-time ASKF (D-ASKF) is applied. The system model is discretized with the two-order truncation error via the Taylor expansion. The CD-ASKF and the CD-TSKF are applied in Case 3 and Case 4, respectively.

The preceding theoretical analysis is conducted in the plane, but simulations are made in a three-dimensional space. The subscripts *e* and *b* are attached to the symbols of physical quantities to denote the elevation loop and the azimuth loop, respectively.

In CD-ASKF and CD-TSKF, with the impact interference estimated, the forces u_2 generated by pulse thrusters, true values and estimates of the additive attitude given as e and $\hat{e}$ in different loops are shown in Fig. 3 and Fig. 4. Note that since the two algorithms are equivalent, the results are the same.

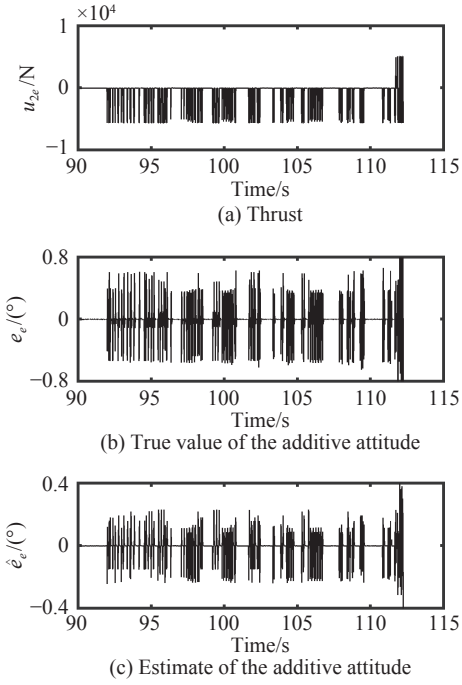

Fig. 3 Thrust, additive attitude and its estimate in elevation loop (CD-ASKF and CD-TSKF)

From Fig. 3 and Fig. 4 one can see similar results happening in both loops. In Fig. 3(b) the true value of the im-

pact interference error varies quickly with the switching on and off of the pulse thrusters. In Fig. 3(c) the estimate of the impact interference error keeps a similar shape to the true value, but the amplitude is not the same as that of the true value. This is because the frequency of the true value is so high that the estimate cannot get up with it for the limitation of the filter's sampling period. If the sampling period can be shortened, the precision of estimation can be improved. The same phenomena can be observed from Fig. 4.

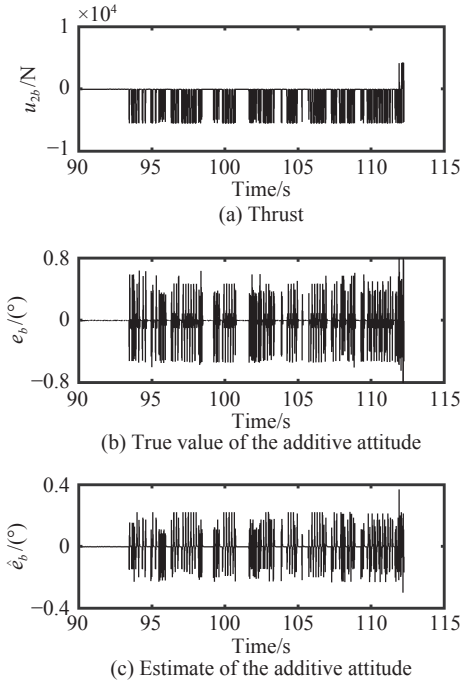

Fig. 4 Thrust, additive attitude and its estimate in azimuth loop (CD-ASKF and CD-TSKF)

The forces generated by pulse thrusters, true values and estimates of the additive attitudes in different loops in D-ASKF are shown in Fig. 5 and Fig. 6. The discretized dynamical model used is not as exact as that in the continuous-discrete filters, so the error is larger and the estimates are quite small.

The introduction of estimating the impact interference is useful for improving the estimation precision of the LOS rate. The estimation results for the LOS rate in the elevation loop under different cases are shown in Fig. 7.

Comparing the results in Fig. 7(a), Fig. 7(b) and Fig. 7(c), one can see that the estimation error of the LOS rate can be reduced when the impact interference has been considered. When the impact inference is ignored (Fig. 7(a)), a vibration with a high frequency occurs in the estimate of the LOS rate, just like the impact interference. But in CD-ASKF and CD-TSKF (Fig. 7(c)), the estimate of LOS rate has tended to a closer neighborhood of the true value. In D-ASKF (Fig. 7(b)), the estimate of additive attitude is less accurate than in continuous-discrete filters as discussed before, so the improvement of the precision of LOS rate is not obvious. The same results can be found from Fig. 8 where the estimation result of the LOS rate in the azimuth loop are shown.

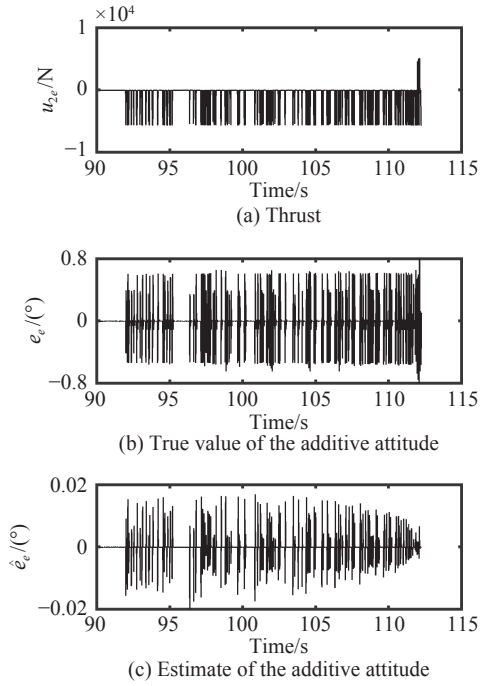

Fig. 5 Thrust, additive attitude and its estimate in elevation loop (D-ASKF)

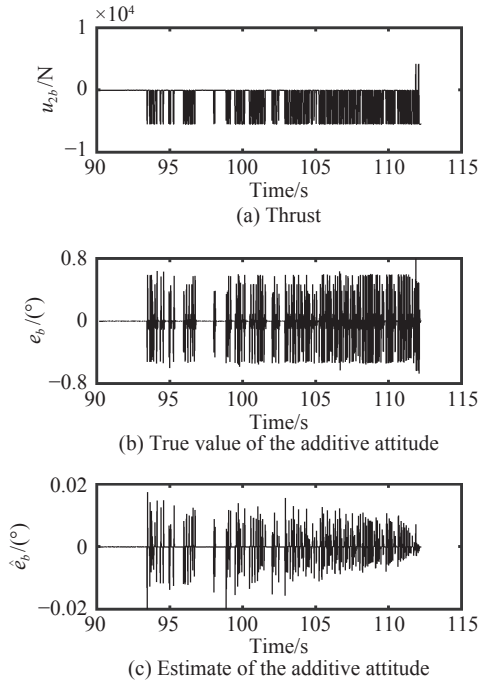

Fig. 6 Thrust, additive attitude and its estimate in azimuth loop (D-ASKF)

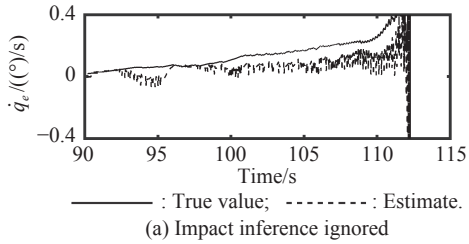

(a) Impact inference ignored

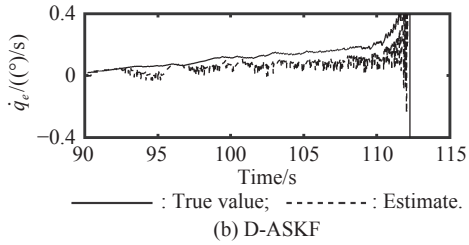

(b) D-ASKF

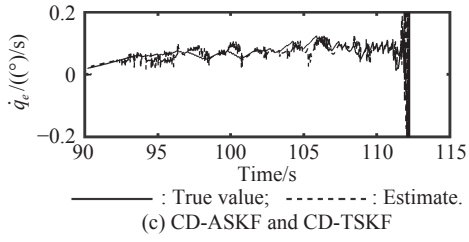

(c) CD-ASKF and CD-TSKF

Fig. 7 LOS rate in elevation loop

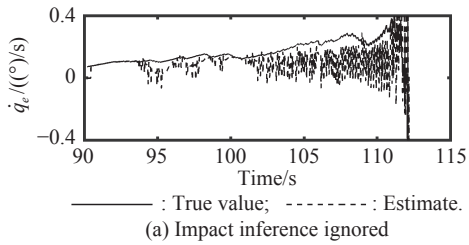

(a) Impact inference ignored

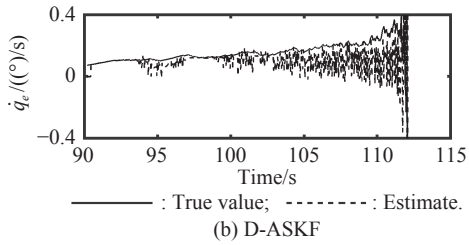

(b) D-ASKF

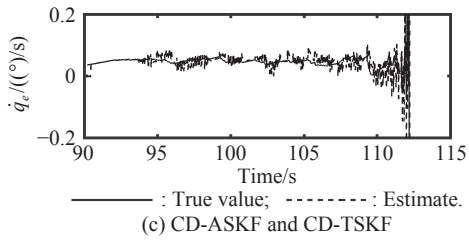

(c) CD-ASKF and CD-TSKF

Fig. 8 LOS rate in azimuth loop

To further prove the effectiveness of the proposed method, the above simulations are conducted 100 times. A statistic result for the 100 runs are shown in Table 1.

Table 1 Statistics of simulation results

Items	Ignore	D-ASKF	CD-ASKF	CD-TSKF
Average miss distance /m	0.774	0.562	0.294	0.294
Average RMSE of pitch LOS rate /(°)/s	0.100	0.083	0.038	0.038
Average RMSE of yaw LOS rate /(°)/s	0.080	0.064	0.036	0.036
Average execution time (one iteration) /ms	0.071	0.110	0.124	0.104

Miss distance measures the performance of the interception. It is defined as the minimum relative distance.

Root mean-squared error (RMSE) measures the accuracy of an estimate. The ith RMSE of an estimate $\hat{\theta}$ given the true value θ is defined as

$$\mathrm{RMSE}_i = \sqrt{\frac{1}{N}\sum_{k=1}^{N}(\hat{\theta}_k - \theta_k)^2} \tag{56}$$

where i represents the ith simulation; θ_k is the true value θ at time t_k; $\hat{\theta}_k$ is the estimate of θ_k; N is the number of estimates.

The results in Table 1 is the averaged RMSE for 100 runs of simulation, i.e.,

$$\overline{\mathrm{RMSE}} = \sum_{i=1}^{100}\mathrm{RMSE}_i$$

Note that at the end of the terminal guidance phase, the LOS rate suddenly diverges, making it impossible to be tracked. Thus, the last few periods of data are omitted when calculating the RMSE_i of the LOS rate.

Execution time of one iteration means average time consumed when the filter calculates an estimate for a new time instant. It describes the computational cost of the filter.

From the statistic result in Table 1, one can see that with the impact interference estimated, the estimation precision of the LOS rate can be improved, and the miss distance can be then reduced. The D-ASKF is the most naive method. The CD-ASKF uses the continuous dynamical model instead of the discretized model with larger error. It reduces the estimation error and consumes more time because of the numerical integration. The CD-TSKF achieves the same performance in estimation error as the CD-ASKF, but reduces the computation time because of the parallel structure and lower-dimension.

Table 2 gives the interval distribution of miss distances. It gives an extra evidence of guidance performance in different cases.

Table 2 Interval distribution of miss distances

Miss distance interval /m	Ignore	D-ASKF	CD-ASKF	CD-TSKF
<0.5	39	56	85	85
<1.0	75	88	100	100
<1.5	90	99	100	100
<2.0	94	100	100	100
<2.5	98	100	100	100
<3.0	100	100	100	100

6. Conclusions

The strong impact interference on the target seeker measurements, caused by the large lateral thrust in the terminal guidance process of a KKV is described with a linear term. The observability of the system consisting of the missile-target relative motion model and the impact interference term has been proven. A method to estimate the impact interference and the LOS rate together via using Kalman filter has been proposed to improve the estimation precision of the LOS rate. In the design of the filter, the continuous-discrete and two-stage techniques have been applied to tackle the time-variant and high-order model issues.

From the simulation result it can been seen that the frequency of the estimate of the impact interference is like that of the true value, although the amplitude is not as high as that of the true value because of the limitation of the sampling period in the filtering algorithm. Since the introduction of the estimation for the impact interference, the estimation for the LOS rate is less affected by the impact interference, so the interception performance of missile is improved. By using the continuous-discrete and two-stage filter techniques, the proposed CD-TSKF increases the estimation accuracy and reduces the computational cost. It shows obvious superiority to the method before.

References

[1] ÖZKAN B, UCAR A. Comparison of the strapdown and gimbaled seekers utilized in aerial applications. Proc. of the Infrared Technology and Applications XXXVIII, 2012. DOI: 10.1117/12.919017.

[2] DU X, XIA Q L. Research on strap-down seeker guidance information for rolling interceptor. Optik, 2017, 129: 183–199.

[3] WALDMANN J. Line-of-sight rate estimation and linearizing control of an imaging seeker in a tactical missile guided by proportional navigation. IEEE Trans. on Control Systems Technology, 2002, 10(4): 556–567.

[4] KRANTHI K R, SANDHYA R, LAXMAN R, et al. LOS rate estimation using extended Kalman filter. Proc. of the International Conference on Emerging Trends in Engineering, 2020: 36–43.

[5] ZHANG G J, YAO Y, MA K M. Line of sight rate estimation of strapdown imaging guidance system based on unscented Kalman filter. Proc. of the 4th International Conference on Machine Learning and Cybernetics, 2005: 1574–1578.

[6] SUN T T, CHU H R, ZHANG B Q, et al. Line-of-sight rate estimation based on UKF for strapdown seeker. Mathematical Problems in Engineering, 2015. DOI: 10.1155/2015/185149.

[7] WANG P, ZHANG K. Research on line-of-sight rate extraction of strapdown seeker. Proc. of the 33rd Chinese Control Conference, 2014: 859–863.

[8] ZHANG Y C, LI J J, LI H Y. Line of sight rate estimation of strapdown imaging seeker based on particle filter. Proc. of the 3rd International Symposium on Systems and Control in Aeronautics and Astronautics, 2010: 191–195.

[9] WEI C Z, HAN Y P, CUI N G, et al. Fifth-degree cubature Kalman filter estimation of seeker line-of-sight rate using augmented-dimensional model. Journal of Guidance, Control, and Dynamics, 2017, 40(9): 2355–2362.

[10] BEST D, PETERSEN C, STERN S, et al. Missile defense: DOD's report provides limited insight on testing options for the ground-based midcourse defense system. Washington DC: Government Accountability Office, 2014.

[11] WHALEN A J, BRENNAN S N, SAUER T D, et al. Observability and controllability of nonlinear networks: the role of symmetry. Physical Review X, 2015, 5(1): 1–18.

[12] SOUTHALL B, BUXTON B F, MARCHANT J A. Controllability and observability: tools for Kalman filter design. Proc. of the British Machine Vision Conference, 1998: 164–173.

[13] KULIKOV G Y, KULIKOVA M V. The accurate continuous-discrete extended Kalman filter for radar tracking. IEEE Trans. on Signal Processing, 2016, 64(4): 948–958.

[14] SÄRKKÄ S. On unscented Kalman filtering for state estimation of continuous-time nonlinear systems. IEEE Trans. on Automatic Control, 2007, 52(9): 1631–1641.

[15] KNUDSEN T, LETH J J. A new continuous discrete unscented Kalman filter. IEEE Trans. on Automatic Control, 2019, 64(5): 2198–2205.

[16] KULIKOV G Y, KULIKOVA M V. NIRK-based Cholesky-factorized square-root accurate continuous-discrete unscented Kalman filters for state estimation in nonlinear continuous-time stochastic models with discrete measurements. Applied Numerical Mathematics, 2020, 147: 196–221.

[17] ARASARATNAM I, HAYKIN S, HURD T R. Cubature Kalman filtering for continuous-discrete systems: theory and simulations. IEEE Trans. on Signal Processing, 2010, 58(10): 4977–4993.

[18] SANTOS-DIAZ E, HAYKIN S, HURD T R. Fifth-degree continuous-discrete cubature Kalman filter for radar. IET Radar, Sonar & Navigation, 2018, 12(11): 1225–1232.

[19] WANG J L, WANG J H, ZHANG D X, et al. Stochastic feedback based Kalman filter for nonlinear continuous-discrete systems. IEEE Trans. on Automatic Control, 2018, 63(9): 3002–3009.

[20] HE R K, CHEN S X, WU H, et al. Adaptive covariance feedback cubature Kalman filtering for continuous-discrete bearings-only tracking system. IEEE Access, 2019, 7: 2686–2694.

[21] KULIKOV G Y, KULIKOVA M V. Accurate state estimation in continuous-discrete stochastic state-space systems with nonlinear or nondifferentiable observations. IEEE Trans. on Automatic Control, 2017, 62(8): 4243–4250.

[22] KULIKOV G Y, KULIKOVA M V. Square-root accurate continuous-discrete extended-unscented Kalman filtering

methods with embedded orthogonal and J-orthogonal QR decompositions for estimation of nonlinear continuous-time stochastic models in radar tracking. Signal Processing, 2020, 166: 107253.

[23] WANG Y H, ZHANG H B, MAO X, et al. Accurate smoothing methods for state estimation of continuous-discrete nonlinear dynamic systems. IEEE Trans. on Automatic Control, 2019, 64(10): 4284–4291.

[24] FRIEDLAND B. Treatment of bias in recursive filtering. IEEE Trans. on Automatic Control, 1969, 14(4): 359–367.

[25] HSIEH C S, CHEN F C. Optimal solution of the two-stage Kalman estimator. IEEE Trans. on Automatic Control, 1999, 44(1): 194–199.

[26] HSIEH C S, CHEN F C. General two-stage Kalman filters. IEEE Trans. on Automatic Control, 2000, 45(4): 819–824.

[27] CHEN X Q, SUN R, JIANG W C, et al. A novel two-stage extended Kalman filter algorithm for reaction flywheels fault estimation. Chinese Journal of Aeronautics, 2016, 29(2): 462–469.

[28] XU J, JING Y, DIMIROVSKI G M, et al. Two-stage unscented Kalman filter for nonlinear systems in the presence of unknown random bias. Proc. of the American Control Conference, 2008: 3530–3535.

[29] CHEN X Q, SUN R, WANG F, et al. Two-stage unscented Kalman filter algorithm for fault estimation in spacecraft attitude control system. IET Control Theory & Applications, 2018, 12(13): 1781–1791.

[30] HAJIYEV C, CILDEN-GULER D, HACIZADE U. Two-stage Kalman filter for fault tolerant estimation of wind speed and UAV flight parameters. Measurement Science Review, 2020, 20(1): 35–42.

[31] LI W. Gaussian mixture PHD filter for multi-sensor multi-target tracking with registration errors. Signal Processing, 2013, 93(1): 86–99.

[32] XU Z, PEI H. Dynamic characteristics analysis of elastic missile. Proc. of the IEEE Chinese Guidance, Navigation and Control Conference, 2017: 98–102.

[33] SONTAG E D. Mathematical control theory: deterministic finite dimensional systems. New York: Springer Science & Business Media, 2013.

[34] STRID I, WALENTIN K. Block Kalman filtering for large-scale DSGE models. Computational Economics, 2009, 33(3): 277–304.

[35] BROWN R G. Introduction to random signal analysis and Kalman filtering. New Jersey: Wiley, 1983.

Biographies

ZHOU Di was born in 1969. He received his B.E. degree and Ph.D. degree in automatic control from Harbin Institute of Technology, Harbin, China, in 1991 and 1996, respectively. He is a professor in School of Astronautics, Harbin Institute of Technology. His research interests include nonlinear control, nonlinear filtering, and guidance and control of missiles.

E-mail: zhoud@hit.edu.cn

HU Zhiheng was born in 1989. He received his M.E. degree in control science and technology from Harbin Institute of Technology in 2014. From 2014 until now, he has been studying in School of Astronautics of Harbin Institute of Technology for his Ph.D. degree. His current research area includes nonlinear filtering, and guidance of missiles.

E-mail: huzhiheng1990@163.com

ZHANG Wenxue was born in 1992. He received his M.S. degree in Control Science and Engineering from Harbin Institute of Technology Shenzhen Graduate School, China, in 2017. From 2017 until now, he has been studying in School of Astronautics of Harbin Institute of Technology for his Ph.D. degree. His current research area is control theory and its applications to flight control systems.

E-mail: wxzhang@hit.edu.cn